JOURNAL OF THERMOPHYSICS AND HEAT TRANSFER
Vol. 17, No. 2, April–June 2003

Laser Ablation of Titanium Metallic Targets: Comparison Between Theory and Experiment

A. Casavola,* G. Colonna,† A. De Giacomo,‡ and M. Capitelli§
University of Bari, 70126 Bari, Italy

A model of plasma expansion with chemical kinetics has been developed and compared with the free-flow model describing the laser ablation plume of metallic titanium target. Optical emission spectroscopy has been used to obtain time of flight (TOF) spectra. The measured shift between Ti and Ti^+ TOF has been theoretically explained on the basis of the recombination process. Particular attention has been also focused on the dependence of TOF on some plume parameters such as initial speed, temperature, pressure, and plume extension.

Nomenclature

a_0	=	Bohr radius
E	=	total energy per unit mass
$F_k(\varepsilon)$	=	energy of the photon emitted in the radiative recombination process
$f(\varepsilon)$	=	electron energy distribution function
H_f	=	formation enthalpy
h	=	Plank constant
K_{eq}	=	ionization equilibrium constant
K_{ion}	=	total ionization rate
$K_{\text{ion},k}$	=	state selected ionization rate
K_{RR}	=	total radiative recombination rate
$K_{\text{RR},k}$	=	state selected radiative recombination rate
$K_{3\text{rec}}$	=	tribody recombination rate coefficient
M	=	mean molar mass
Ns	=	number of species
n	=	principal quantum number
n_k	=	population of the kth atomic energy level
P	=	pressure
P_0	=	initial pressure of the plume
Q_e	=	total energy emission velocity by radiative recombination
R	=	gas constant
R_{RR}	=	total radiative recombination energy emission rate
$R_{\text{RR},k}$	=	state selected radiative recombination energy emission rate
Ry	=	Rydberg constant
T	=	gas temperature
T_0	=	initial gas temperature
t	=	time from the laser pulse
$t_{\max}$	=	time corresponding to the maximum of the time of flight peak
U	=	internal energy
u	=	flow speed
$v(\varepsilon)$	=	electron speed
v_0	=	initial velocity of the plume
$[X]$	=	particle concentration of the x species
$[X]_{\max}$	=	maximum particle concentration of the x species
x	=	distance from the target
x_0	=	initial width of the plume profile
Z	=	ion charge
ε	=	electron energy
θ	=	dispersion angle with respect to the normal at the surface
ρ	=	total density
ρ_i	=	density of the ith species
$\sigma_{\text{ion},k}(\varepsilon)$	=	electron impact ionization cross section from the atomic state k
$\sigma_{\text{RR},k}(\varepsilon)$	=	radiative recombination cross section in the atomic state k

Received 14 August 2002; revision received 1 December 2002; accepted for publication 2 December 2002.

*Research Fellow, Dipartimento di Chimica and Bari sector CNR–IMIP, via Orabona number 4; cscpac62@area.ba.cnr.it.

†Senior Researcher, Dipartimento di Chimica and Bari sector CNR–IMIP, via Orabona number 4; gp.colonna@area.ba.cnr.it. Member AIAA.

‡Research Fellow, Dipartimento di Chimica and Bari sector CNR–IMIP, via Orabona number 4; adg@centrolaser.it.

§Professor, Dipartimento di Chimica and Bari sector CNR–IMIP, via Orabona number 4; m.capitelli@area.ba.cnr.it. Member AIAA.

Introduction

THE study of laser-induced plasma (LIP) plays a fundamental role for diagnostic purposes in many applications, concerning laser–matter interaction: pulsed-laser deposition (PLD), laser induced breakdown spectroscopy, laser welding, laser cutting, and so on.[1–7] The flexibility of the experimental setup and the large quantity of condensed matter material that can be treated by laser make PLD a very promising technique for thin-film production. For example, plasma-assisted PLD has been successfully used for growing TiO_2 thin films.[1]

Recently, laser ablation has been studied as an interesting micropropulsion technique.[8–13] The advantages of laser thrusters are the simplicity of the apparatus, the high-energy efficiency, and the precise thrust control. These characteristics make ablative laser propulsion a good tool for satellite applications.[8–13]

In the last 10 years, a large number of experimental and theoretical works[14–16] were devoted to LIP generation and evolution; nevertheless, these processes are still not well understood. The interpretation of experimental results can be improved by theoretical modeling of the plume expansion. Many models have been developed based on the solution of the one-dimensional Euler equation (see Refs. 17 and 18) in the frozen-flow approximation. The validity of the one-dimensional approach has been proved in Refs. 17 and 18, where angular dispersion is of the order of $\cos^{30}\theta$, whereas the frozen-flow assumption could be open to question. The model has been improved for a TiO plume by including chemical reactions in the local thermodynamic equilibrium (LTE) approximation. Nevertheless, the comparison between theoretical and experimental results is only qualitative. The discrepancies are due to many factors such as chemical model and initial conditions that are strictly coupled to each other, due to the strong nonlinearity in the equations.

Similarities with high-enthalpy nozzle expansion[19] lead to the conclusion that strong nonequilibrium can be present, mainly in the expansion zone. Therefore, a kinetic model is necessary to describe properly the flow properties.

In this paper we will investigate how the chemical models as well as the initial conditions of the plume affect the plume expansion. In particular our attention is focused on the time of flight (TOF) diagram that can be directly related to experimental measurements in vacuum.

Theoretical Model

Euler Equations

The theoretical model basically describes the plume expansion using fluid dynamic equations along the plume axis in the one-dimensional approximation, based on the observation that the angular dispersion of the plume is small.[17,18] Euler equations consist of mass, momentum, and energy continuity equations:

$$\frac{\partial \rho_i}{\partial t} + \frac{\partial \rho_i u}{\partial x} = 0 \tag{1}$$

$$\frac{\partial \rho u}{\partial t} + \frac{\partial (\rho u + P)}{\partial x} = 0 \tag{2}$$

$$\frac{\partial \rho E}{\partial t} + \frac{\partial \rho u E}{\partial x} + P\frac{\partial u}{\partial x} = 0 \tag{3}$$

completed with an equation to calculate the total density ρ,

$$\rho = \sum_{i=1}^{Ns} \rho_i \tag{4}$$

and the ideal gas state equation,

$$P = (P/\bar{M})RT \tag{5}$$

The general expression of total energy per unit mass, E, is

$$E = \tfrac{3}{2}(RT/\bar{M}) + U/\bar{M} + H_f/\bar{M} \tag{6}$$

For an ideal gas without internal structure and chemical reactions, Eq. (5) is simplified as

$$P = \tfrac{2}{3}\rho E \tag{7}$$

Solution of the system of equations (1–6) allows calculating the time-dependent profiles of different macroscopic quantities, such as mass density, temperature, and Mach number along the distance between the target and the substrate.

The laser evaporation mechanisms are very complex and depend on the surface characteristics. For nanosecond laser pulses, the use of analytical models is reasonable because the high pressure reached in the plume at a very short time thermalizes the plasma and the memory of the evaporation mechanism is lost. We have considered two analytical approximated models for the target evaporation[17,18]: 1) The plume is evaporated in a very short time [instantaneous evaporation approximation (IEA)] and expands after this production. 2) The plume is produced in a given time interval simulating the evaporation [continuous evaporation approximation (CEA)]. The evaporation models are determined by fixing some parameters that define the initial conditions. Such parameters depend on the analytical model considered, and for the two cases can be summarized as follows: 1) for IEA, the initial profile of pressure, temperature, speed, and plume extension and 2) for CEA the flux of mass, momentum and energy from the surface, and the composition of the evaporated matter.

These values cannot be determined experimentally due to the strong continuum emission and, therefore, must be guessed to have a good agreement with experimental data available at longer times. To study the effects of the initial parameters on the plume expansion, we have performed a sensitivity analysis of the flow properties to parameter variations.[20] In the present paper we discuss only the results obtained by the IEA model.

Chemical Kinetics Model

We have considered two different models to include reactions in the fluid dynamic code. In the LTE approximation, we couple the fluid dynamic equations with the chemical equilibrium model.[21,22] In this case, the gas composition and all of the thermodynamic functions depend on the local temperature and pressure only or, equivalently, on total density and energy. This approach has been recently applied to the plume formed when a titanium monoxide (TiO) target is ablated.[22]

Some experimental[23] and theoretical[24] results lead to the conclusion that the LTE approximation cannot be applied during the plume expansion at low pressure and that a kinetic approach should be used. To investigate the effects of finite rate coefficients on the plume expansion, the following processes[25] have been considered: 1) ionization by electron impact (direct process), 2) three-body recombination (inverse process)

$$\mathrm{Ti}_k + e^-(\varepsilon) \leftrightarrow \mathrm{Ti}^+ + 2e^- \tag{8}$$

and 3) radiative recombination

$$\mathrm{Ti}^+ + e^-(\varepsilon) \leftrightarrow \mathrm{Ti}_k + h\nu \tag{9}$$

where the index k refers to the internal energy level of the atom involved in the processes (8) and (9).

The cross sections $\sigma_{\mathrm{ion},k}(\varepsilon)$ of the ionization process [Eq. (8)] have been calculated using the classical Grizinskii approach[26] from each internal level and for a wide range of the electron energy. The ionization rate coefficients $K_{\mathrm{ion},k}$ from a given level k have been calculated by integrating the relevant cross sections over a Maxwellian electron energy distribution function f (Ref. 27)

$$K_{\mathrm{ion},k} = \int_0^\infty f(\varepsilon) v(\varepsilon) \sigma_{\mathrm{ion},k}(\varepsilon)\, \mathrm{d}\varepsilon \tag{10}$$

The total ionization rate coefficients K_{ion} have been calculated summing the state selected rate coefficient [Eq. (10)] over a Boltzmann internal level distribution n_k at the same temperature as the free electrons[27]

$$K_{\mathrm{ion}} = \sum_k K_{\mathrm{ion},k} n_k \tag{11}$$

The rate coefficients obtained in this way depend only on one temperature, and the results have been fitted by the following analytical expression and have been reported in Fig. 1:

$$K_{\mathrm{ion}} = \exp\left(27.809 - \frac{T}{9417.6} - \frac{80102}{T+1}\right) \tag{12}$$

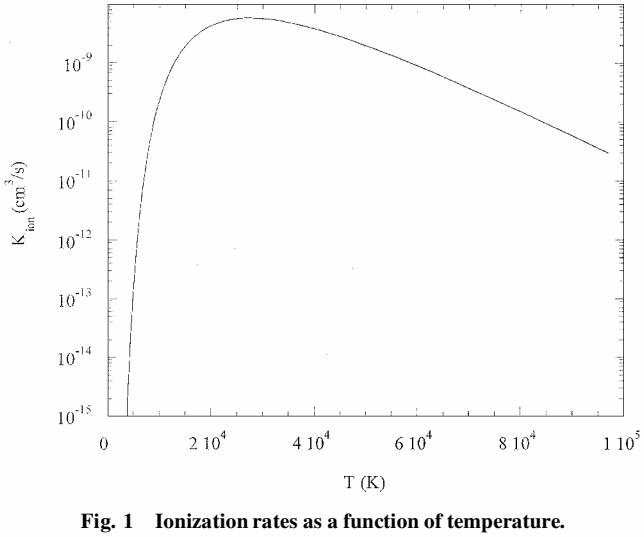

Fig. 1 Ionization rates as a function of temperature.

The three-body recombination rates K_{3rec} have been calculated by detailed balance principle:

$$K_{3rec} = K_{ion}/K_{eq} \tag{13}$$

In turn, the ionization equilibrium constant, calculated according to statistical thermodynamics,[28] has been fitted as a function of temperature with the following law:

$$K_{eq} = 1.11\cdot 10^{-16} - 8.41\cdot 10^{-20}T + 4.38\cdot 10^{-24}T^2 + 1.93\cdot 10^{-29}T^3 \tag{14}$$

The radiative recombination cross section $\sigma_{RR,k}(\varepsilon)$ on level k has been calculated in the hydrogenlike atom approximation[29]:

$$\sigma_{RR,k}(\varepsilon) = \pi a_0^2 \frac{32Z^4 Ry^2}{3\sqrt{3}(137)^3 F_k(\varepsilon) n^3 \varepsilon} \tag{15}$$

The radiative recombination rate on level k is calculated by integrating the cross section [Eq. (15)] over the electron energy distribution $f(\varepsilon)$:

$$K_{RR,k} = \int_0^\infty f(\varepsilon) v(\varepsilon) \sigma_{RR,k}(\varepsilon)\, d\varepsilon \tag{16}$$

approximated with a Maxwellian. To obtain the total radiative recombination rate, we have summed over all of the atomic levels,

$$K_{RR} = \sum_k K_{RR,k} \tag{17}$$

The results have been interpolated by the function (Fig. 2)

$$K_{RR} = \exp\left\{19.905 - 0.452\cdot \ell n(T) - 0.013993\cdot \exp\left[\frac{\ell n(T)}{2.419}\right]\right\} \tag{18}$$

The radiative recombination converts electron translational energy in electromagnetic energy (continuous emission light). The energy emission rate for ions recombining on atomic level k is given by

$$R_{RR,k} = \int_0^\infty f(\varepsilon) v(\varepsilon) \sigma_{RR,k}(\varepsilon) F_k(\varepsilon)\, d\varepsilon \tag{19}$$

and the total emission rate is given by the sum over all of the atomic levels

$$R_{RR} = \sum_k R_{RR,k} \tag{20}$$

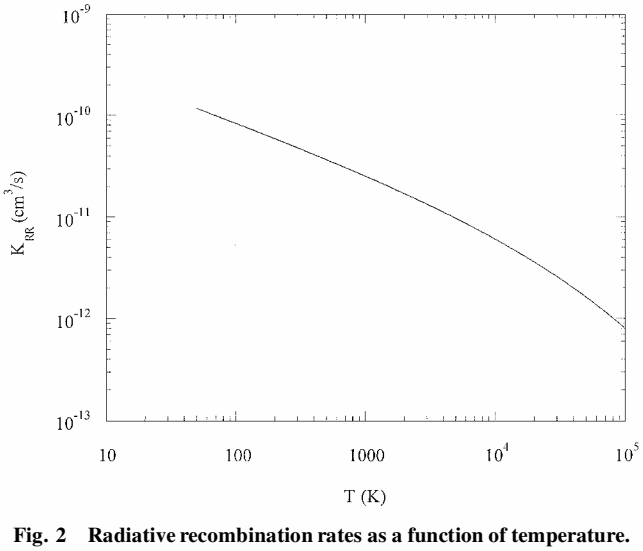

Fig. 2 Radiative recombination rates as a function of temperature.

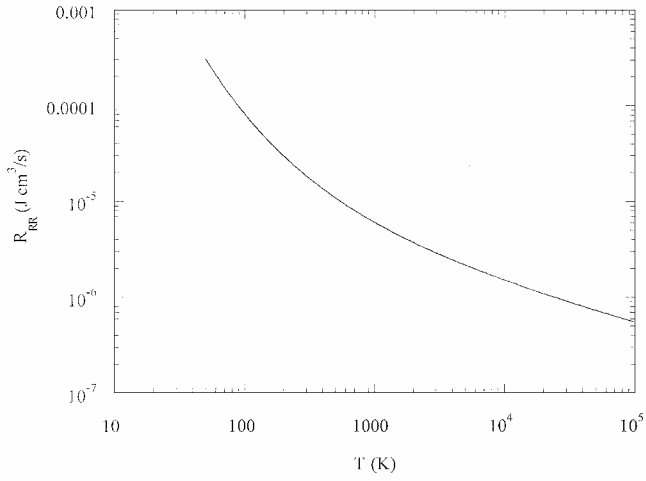

Fig. 3 Rate of energy emission due to radiative recombination as a function of temperature.

and the total irradiated energy per time unit and volume unit (joules per cubic meter per second) is given by

$$Q_e = [e^-]\cdot[Ti^+]\cdot R_{RR} \tag{21}$$

The rate of emission energy (in joules cubic meters per mol squared per second) due to radiative recombination can be fitted by the analytical expression (Fig. 3)

$$R_{RR} = \exp\left\{30.663 - 0.36556\cdot \ell n(T) + 26.609\cdot \exp\left[-\frac{\ell n(T)}{1.9606}\right]\right\} \tag{22}$$

To take into account the loss of energy due to the radiative recombination, Eq. (3) has been modified as

$$\frac{\partial \rho E}{\partial t} + \frac{\partial \rho u E}{\partial x} + P\frac{\partial u}{\partial x} = -Q_e \tag{23}$$

We can calculate the time evolution concentrations of different species by means of the following equations derived by classical chemical kinetics theory:

$$\frac{d[Ti]}{dt} = -K_{ion}[Ti][e^-] + K_{3rec}[Ti^+][e^-][e^-] + K_{RR}[Ti^+][e^-] \tag{24}$$

$$\frac{d[Ti^+]}{dt} = K_{ion}[Ti][e^-] - K_{3rec}[Ti^+][e^-][e^-] - K_{RR}[Ti^+][e^-] \tag{25}$$

$$\frac{d[e^-]}{dt} = K_{ion}[Ti][e^-] - K_{3rec}[Ti^+][e^-][e^-] - K_{RR}[Ti^+][e^-] \tag{26}$$

The coupling between fluid dynamic and kinetic equations involves an "operator splitting" technique: As a first step, we solve the Euler equations in the free-flow approximation,[22] and then in the same time interval, we solve the kinetic equations locally to update the concentration and total energy values.[20,30] This approach is valid for small temperature variations.

Experimental Approach

TOF measurements allow studying the dynamic aspects of LIP and give important information on the temporal evolution of species in the plume. Different experimental techniques can be employed for this propose, among them the most widely used are optical emission spectroscopy (OES),[31,32] laser-induced fluorescence,[33] laser absorption, probing,[34] and mass spectrometry.[35] Charged particles detection and laser excitation techniques give the best results for what

concerns the investigation of LIP far from the target, but OES is the simplest way to do TOF measurements in the high brightness zone of LIP (0–3 mm).

For this reason, we perform the study of evolution of LIP species by temporally and spatially resolved OES at different distance from the target. Two nonresonance lines have been selected, 399.86 and 401.23 nm, corresponding to the species Ti and Ti^+, respectively. These lines have been chosen because the corresponding emission time is shorter than the plasma expansion time. Moreover, the selected lines have closed spectral positions and similar energy.

The experimental setup has been described in details in previous work[31] and consists of a vacuum chamber with rotating holder for target and quartz windows for laser input and for the emission spectra detection, a spectroscopic system and a vacuum system. The laser source is a KrF excimer laser at 248 nm (Lambda Physic LPX350) with a pulse width of 30 ns and an adjustable repetition rate between 1 and 150 Hz. By the use of a mirror and lens, the laser beam is directed through a quartz window into the vacuum chamber and focused onto the target at 45 deg from the surface normal. In these experiments, the energy density of the laser beam has been fixed at 5 J/cm^2 with a rectangular spot 2.00×2.42 mm^2 and a repetition rate of 5 Hz.

The spectroscopic system is made by an optical fiber (diameter of 0.6 mm) connected to the input slit of an high-resolution monochromator (HR 640, Instruments, S.A., division Jobin Yvon) and an intensified charge-coupled device (ICCD) (Jobin Yvon cv3000) for the detection of spectra. The plume image is focused on a virtual plane by a short focus quartz lens (6 cm). The optical fiber is placed on a micrometric XYZ table so that it is possible to move the entrance of the optical fiber in the virtual plane, where is focused the plume image with a 1:1 magnitude. This configuration allows detecting a portion of plume with a spatial resolution that has the same dimension of the optical fiber entrance. The signal of a fast photodiode, detecting the laser reflection of the diaphragm, is the main trigger for the ICCD. To avoid the intrinsic delay of the electronic system (80 ns) a 25-m-long optical fiber is used so that the transmission of emission light to the detection system is delayed of 83 ns as measured by a fast oscilloscope. A gate width of 40 ns has been chosen in the experiment to maximize the spectral line intensity while maintaining a good temporal resolution. To optimize the signal-to-noise ratio and the spectra reproducibility, the detection of spectra is carried out averaging 5 sets of 10 signal accumulations. By this acquisition mode, the fluctuations of spectra are under 7% at the experimental conditions applied in this work.

The spectroscopic investigation of the LIP has been carried on in the visible range at the maximum vacuum allowed by our vacuum system 10^{-6} torr. To neglect the angular dispersion of LIP, the measurements have been performed along the propagation axis at distances from the target surface shorter or comparable to the spot dimension.[36]

Results and Discussion

To compare systematically theoretical and experimental results, it is necessary to define accurately the initial conditions. In this way, when v_0, P_0, T_0, and x_0 are changed alternatively, it is possible to find the initial conditions that are the best fit for experimental data (see also Ref. 20).

Let us discuss the role of the different parameters in affecting the plume properties. Figure 4 shows the dependence of TOF on v_0 variations. Inspection of Fig. 4 shows that times at which Ti concentrations reach their maximum decrease with increasing v_0. At the same time, the broadening of the peaks follows a similar trend.

Figures 5 and 6 show the effect of the pressure. In particular Fig. 5 shows the time evolution of titanium concentration for different pressure values. Notice that the concentration of titanium increases with increasing the pressure due to the corresponding increase in the recombination rates. After normalizing the TOF to their maximum (Fig. 6), we can appreciate the shift and the broadening of the peaks to pressure variations.

More relevant is the effect of changing the initial temperature, as shown in the plots of normalized titanium atom and ion

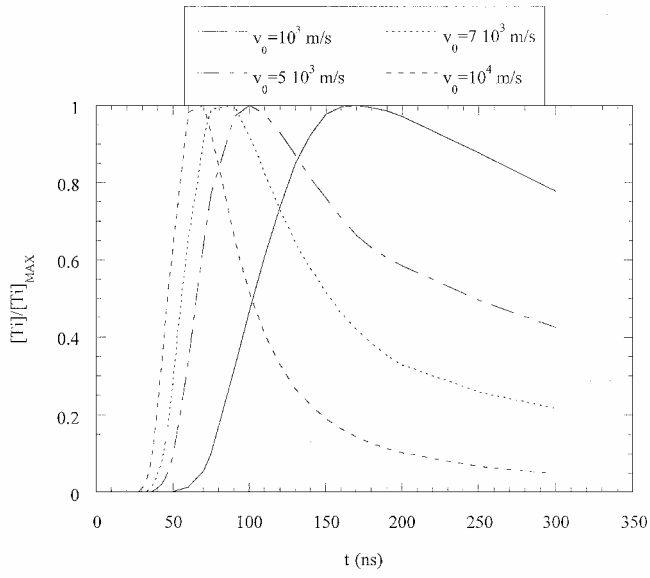

Fig. 4 Normalized atomic concentrations as a function of time at $x = 0.6$ mm from the target at different initial velocities v_0, for $P_0 = 20$ atm, $T_0 = 20{,}000$ K, and $x_0 = 0.05$ mm.

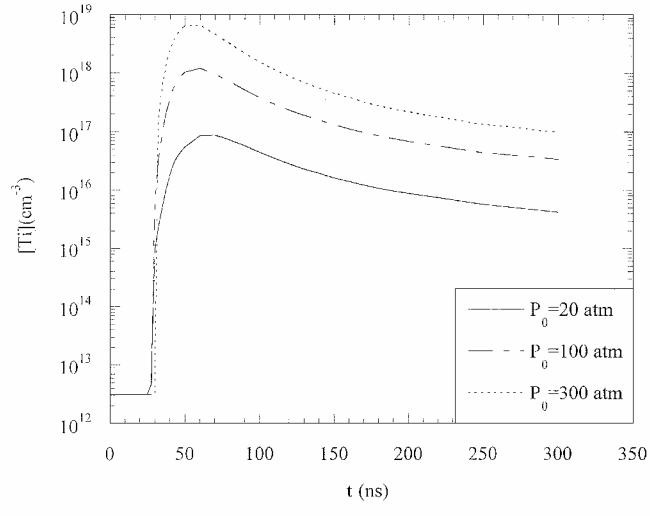

Fig. 5 Atomic concentrations as a function of time at $x = 0.6$ mm from the target at different initial pressures P_0, for $v_0 = 10^4$ m/s, $T_0 = 20{,}000$ K, and $x_0 = 0.05$ mm.

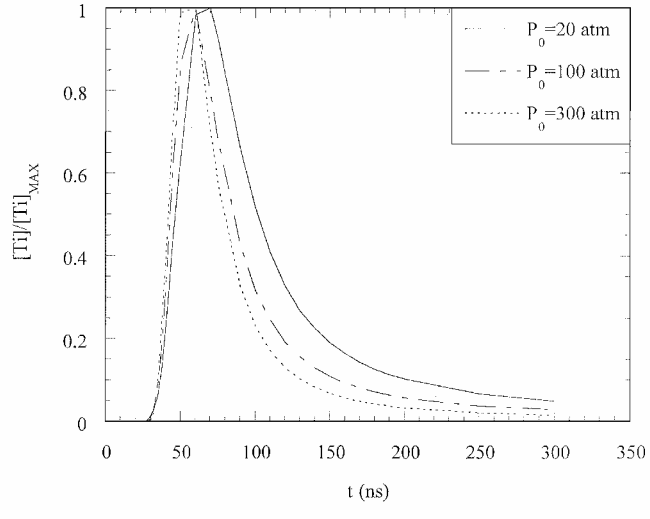

Fig. 6 Normalized atomic concentrations as a function of time at $x = 0.6$ mm from the target at different initial pressures P_0, for $v_0 = 10^4$ m/s, $T_0 = 20{,}000$ K, and $x_0 = 0.05$ mm.

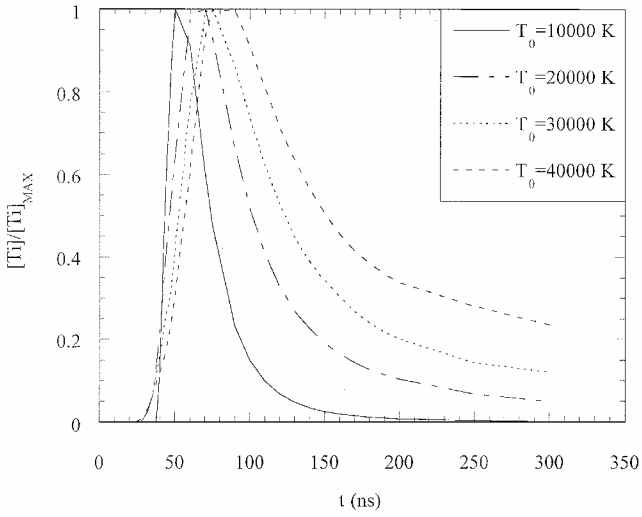

Fig. 7 Normalized atomic concentrations as a function of time at $x = 0.6$ mm from the target at different initial temperatures, for $v_0 = 10{,}000$ m/s, $P_0 = 20$ atm, and $x_0 = 0.05$ mm.

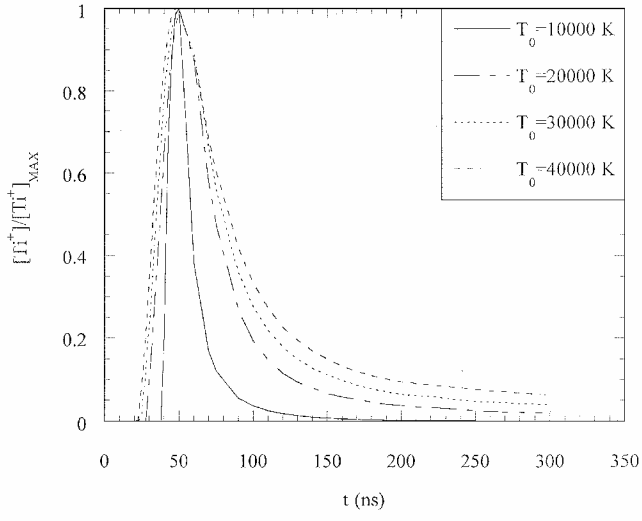

Fig. 8 Normalized ion concentrations as a function of time at $x = 0.6$ mm from the target at different temperatures, for $v_0 = 10{,}000$ m/s, $P_0 = 20$ atm, and $x_0 = 0.05$ mm.

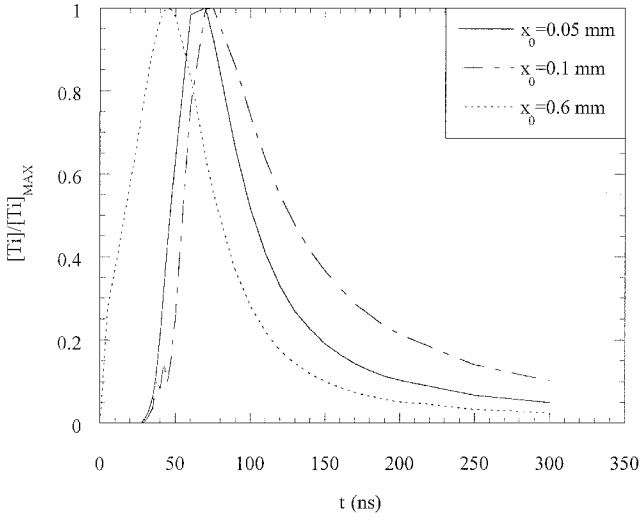

Fig. 9 Atomic normalized concentrations as a function of time at $x = 0.6$ mm from the target at different initial plume extension x_0, for $v_0 = 10{,}000$ m/s, $P_0 = 20$ atm, and $T_0 = 20{,}000$ K.

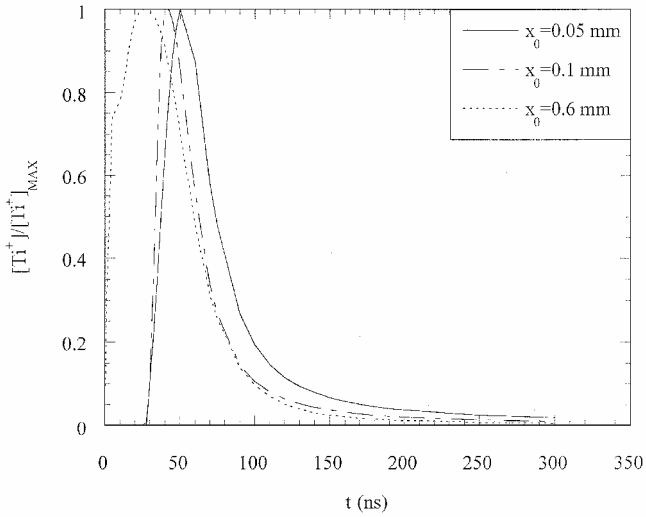

Fig. 10 Ion normalized concentrations as a function of time at $x = 0.6$ mm from the target at different initial plume extension x_0, for $v_0 = 10{,}000$ m/s, $P_0 = 20$ atm, and $T_0 = 20{,}000$ K.

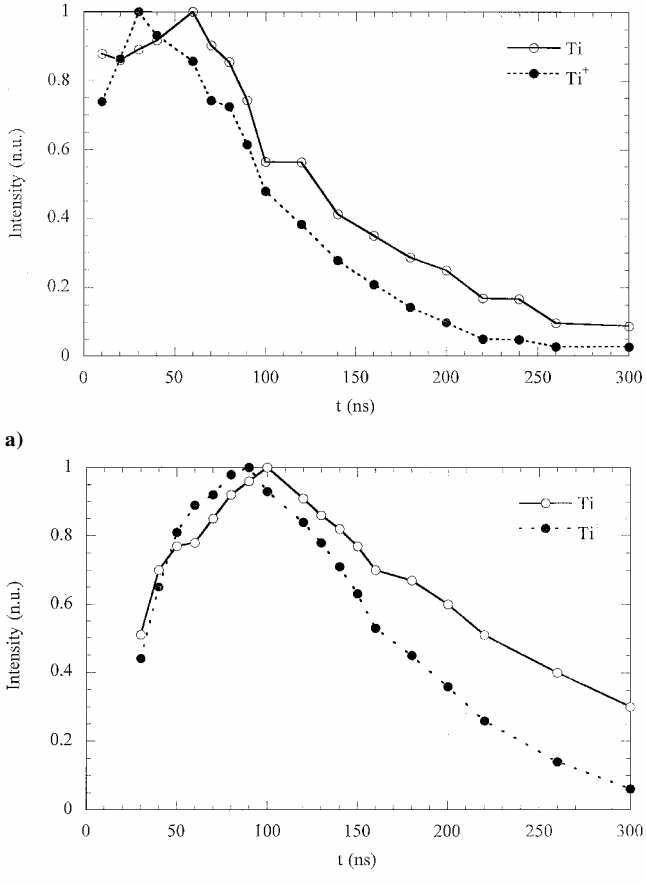

Fig. 11 Experimental TOF of Ti and Ti^+ species at a) 0.5 mm and b) 1 mm.

concentration (Figs. 7 and 8): In both cases there is a broadening of the peaks as the temperature increases. Whereas in Fig. 8 the maximum is fixed at about 50 ns, in the case of atom concentration there is a shift of the peak at a longer time. This shift is due to recombination. In fact, when the initial temperature is high, the initial concentration of Ti is very low and the recombination effect is much more evident.

Figures 9 and 10 show the dependence of Ti and Ti^+ TOF for both Ti and TiIt on the initial extension of the plume x_0. Again note that the TOF profiles strongly depend on the x_0 value.

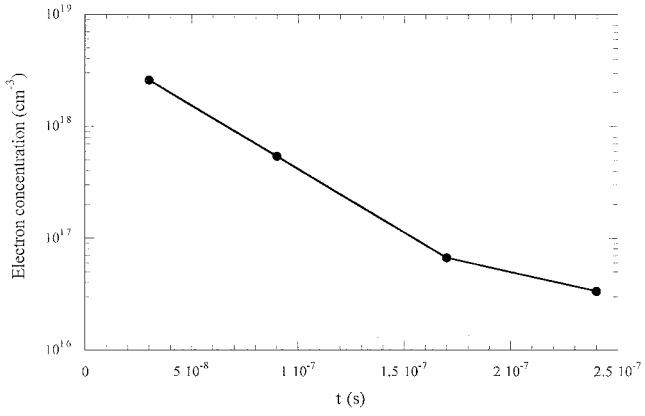

Fig. 12 Experimental temporal evolution of electron number density.

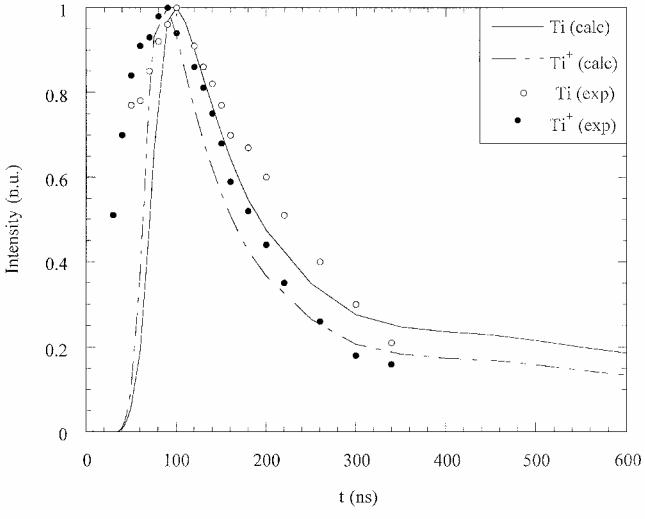

a)

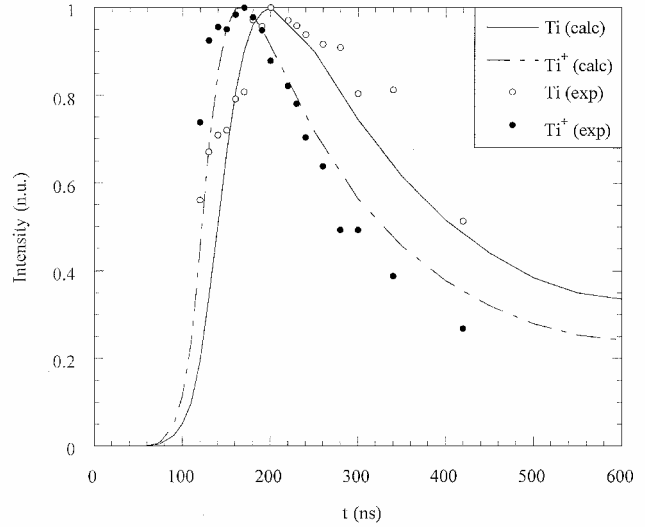

b)

Fig. 13 Examples of the comparison between experimental and calculated TOF with theoretical initial conditions $v_0 = 7000$ m/s, $P_0 = 20$ atm, $T_0 = 20{,}000$ K, and $x_0 = 0.15$ mm for a) 1 mm and b) 2 mm.

Let us now compare the results of the model with the corresponding experimental ones. Figures 11a and 11b show the normalized TOF for Ti and Ti$^+$ at 0.5 and 1 mm from the target obtained experimentally by OES. We can see that in both cases the peaks corresponding to the Ti TOF present a delay in respect to the corresponding one for the Ti$^+$. This delay can be attributed to the three-body recombination mechanism. The plasma under study is in fact in the recombination phase, that is, in the kinetic expression

Table 1 Time corresponding to the maximum of experimental and calculated TOF. The error is determined as the temporal difference between following points

	t_{max} Ti (ns)		t_{max} Ti$^+$ (ns)	
x (mm)	exp	calc	exp	calc
0.5	60 ± 10	45 ± 0.5	30 ± 10	42 ± 0.5
1.0	100 ± 10	100 ± 10	90 ± 10	90 ± 10
2.0	200 ± 10	200 ± 10	170 ± 10	170 ± 10
3.0	360 ± 30	300 ± 50	280 ± 30	250 ± 50

$$\frac{d[e^-]}{dt} = K_{ion}[e^-][Ti] - K_{3rec}[e^-]^3 \qquad (26)$$

the recombination term is predominant. This point is also supported by the experimental trend of electron number density vs time (see Fig. 12) determined by Stark broadening from the emission spectrum corresponding to the maximum of TOF signal at different distances. Inspection of Fig. 12 shows that $d[e^-]/dt < 0$, thus, indicating the prevalence of the recombination mechansm.[37]

Figures 13a and 13b show a comparison between experimental and theoretical results for Ti and Ti$^+$ TOF at 1 and 2 mm. We can observe a satisfactory agreement at all of the distances examined in this work. Some differences arise after 2 mm as a consequence of the radial component of velocity and the experimental curves are broader than the theoretical ones. Table 1 lists the time corresponding to the maximum of TOF curves obtained by experiments and by calculation for Ti and Ti$^+$ species at different distances. The quantitative agreement of Table 1 is a confirmation of the effect of the three-body recombination on temporal evolution of LIP and it proves the validity of theoretical method adopted in this work.

Conclusions

A theoretical investigation of the plume expansion using different chemical models has been presented. We have investigated a wide range of initial conditions by changing alternatively different initial parameters. A systematic study of the effect of all of these parameters on the plume expansion has been done. A good agreement between theoretical and experimental results has been found.

Future improvement of the model will be directed in two directions. The first one is the insertion of a collisional-radiative model for the internal states of Ti and Ti$^+$ species. The second direction will try to develop an authomatic tool for predicting the best initial conditons for reproducing the experimental TOF. Work is under study in both directions.

Acknowledgments

This work has been partially supported by CNR/P.F. Materiali Speciali per Tecnologie Avanzate (Contract 97.01005.34), Cofin. MIUR 2001031223_009, and PON–TECSIS(MIUR).

References

[1]De Giacomo, A., Shakhatov, V. A., Senesi, G. S., De Pascale, O., and Prudenzano, F., "Plasma Assisted Pulsed Laser Deposition for the Improvement of the Film Growth Process," *Applied Surface Science*, Vol. 186, No. 1–4, 2002, pp. 533–537.

[2]Teghil, R., D'Alessio, L., Santagata, A., Zaccagnino, M., and Ferro, D., "Pulsed Laser Ablation of MoSi2: Gas Phase Analysis," *Applied Surface Science*, Vol. 186, No. 1–4, 2002, pp. 335–338.

[3]Cappelli, E., Orlando, S., Mattei, G., Pinzari, F., and Zoffoli, S., "RF-Plasma Assisted Pulsed Laser Deposition of Carbon Films from Graphite Target," *Applied Surface Science*, Vol. 186, No. 1–4, 2002, pp. 441–447.

[4]Teghil, R., D'Alessio, L., Zaccagnino, M., Ferro, D., Marotta, V., and De Maria, G., "TiC and TaC Deposition by Pulsed Laser Ablation: A Comparative Approach," *Applied Surface Science*, Vol. 173, No. 3–4, 2001, pp. 233–241.

[5]Giardini Guidoni, A., Flamini, C., Varsano, F., Ricci, M., Teghil, R., Marotta, V., and Di Palma, T. M., "Ablation of Transition Metal Oxides by Different Laser Pulse Duration and Thin Films Deposition," *Applied Surface Science*, Vol. 154–155, 2000, pp. 467–472.

[6]Chrisey, D. B., and Huber, G. K., "Mechanisms of Pulsed Laser Sputtering," *Pulsed Laser Deposition of Thin Films*, Wiley-Interscience, New York, 1994, pp. 55–87.

[7]Sadoqi, M., Kumar, S., and Yamada, Y., "Photochemical and Photothermal Model for Pulsed-Laser Ablation," *Journal of Thermophysics and Heat Transfer*, Vol. 16, No. 2, 2002, pp. 193–199.

[8]Pakhomov, A. V., Thompson, M. S., and Gregory, D. A., "Ablative Laser Propulsion Efficiency," AIAA Paper 2002-2157, May 2002.

[9]Ziemer, J. K., "Laser Ablation Microthruster Technology," AIAA Paper 2002-2153, May 2002.

[10]Pakhomov, A. V., and Gregory, D. A., "Ablative Laser Propulsion: An Old Concept Revisited," *AIAA Journal*, Vol. 38, No. 4, 2000, pp. 725–727.

[11]Pakhomov, A. V., Thompson, M. S., and Gregory, D. A., "Specific Impulse and Other Characteristics of Elementary Propellants for Ablative Laser Propulsion," *AIAA Journal*, Vol. 40, No. 5, 2002, pp. 947–952.

[12]Pakhomov, A. V., Thompson, M. S., Gregory, D. A., and Swift, W., Jr., "Specific Impulse Study of Ablative Laser Propulsion," AIAA Paper 2001-3663, July 2001.

[13]Pakhomov, A. V., Thompson, M. S., and Gregory, D. A., "Ablative Laser Propulsion: Specific Impulse and Thrust Derived from Force Measurements," *AIAA Journal* (submitted for publication).

[14]Amoruso, S., "Modelling of UV Pulsed Laser Ablation of Metallic Target," *Applied Physics A: Material Science and Processing*, Vol. 69, Supplement, 1999, pp. 323–332.

[15]Singh, R. K., and Narayan, J., "Pulsed-Laser Evaporation Technique for Deposition of Thin Films: Physics and Theoretical Model," *Physical Review B*, Vol. 41, No. 13, 1990, pp. 8843–8859.

[16]Urbassek, H. M., and Michl, J., "A Gas-Flow Model for the Sputtering of Condensed Gases," *Nuclear Instruments and Methods in Physics Research, Section B*, Vol. 22, No. 4, 1987, pp. 480–490.

[17]Kelly, R., "Gas Dynamics of the Pulsed Emission of a Perfect Gas with Applications to Laser Sputtering and to Nozzle Expansion," *Physical Review A: General Physics*, Vol. 46, No. 2, 1992, pp. 860–874.

[18]Kelly, R., and Miotello, A., "Pulsed Laser Sputtering of Atoms and Molecules, Part I: Basic Solutions for Gas Dynamic Effects," *Applied Physics B: Photophysics and Laser Chemistry*, Vol. B57, No. 2, 1993, pp. 145–158.

[19]Colonna, G., Tuttafesta, M., Capitelli, M., and Giordano, D., "NO Formation in One-Dimensional Nozzle Airflow with State-to-State Nonequilibrium Vibrational Kinetics," *Journal of Thermophysics and Heat Transfer*, Vol. 13, No. 3, 1999, pp. 372–375.

[20]Casavola, A., Colonna, G., and Capitelli, M., "Non Equilibrium Conditions During a Laser Induced Plasma Expansion," *Applied Surface Science* (to be published).

[21]Colonna, G., Casavola, A., and Capitelli, M., "On the Modeling of TiO Plume Expansion Under Laser Ablation," *ALT '99 International Conference on Advanced Laser Technologies*, edited by V. I. Pustovoy and V. I. Konov, Proceedings of SPIE, Vol. 4070, Society of Photo-Optical Instrumentation Engineers, Bellingham, WA, 2000, pp. 293–299.

[22]Colonna, G., Casavola, A., and Capitelli, M., "Modelling Plasma LIBS Expansion," *Spectrochimica Acta Part B: Atomic Spectroscopy*, Vol. 56, No. 6, 2001, pp. 567–586.

[23]De Giacomo, A., Shakhatov, V. A., and De Pascale, O., "Optical Emission Spectroscopy and Modeling of Plasma Produced by Laser Ablation of Titanium Oxides," *Spectrochimica Acta Part B: Atomic Spectroscopy*, Vol. 56, No. 6, 2001, pp. 753–776.

[24]Colonna, G., Pietanza, L. D., and Capitelli, M., "Coupled Solution of a Time-Dependent Collisional-Radiative Model and Boltzmann Equation for Atomic Hydrogen Plasmas: Possible Implication with LIBS Plasma," *Spectrochimica Acta Part B: Atomic Spectroscopy*, Vol. 56, No. 6, 2001, pp. 587–598.

[25]Colonna, G., Casavola, A., Pietanza, L. D., De Giacomo, A., Shakhatov, V. A., and Capitelli, M., "Experimental and Theoretical Investigation of Nonequilibrium In Laser Induced Plasmas," AIAA Paper 2001-2806, June 2001.

[26]Gryzinski, M., "Two-Particle Collisions. I. General Relations for Collisions in the Laboratory System," *Physical Review*, Vol. 138, No. 2A, 1965, pp. A305–A321.

[27]Colonna, G., and Capitelli, M., "Self-Consistent Model of Chemical, Vibrational, Electron Kinetics in Nozzle Expansion," *Journal of Thermophysics and Heat Transfer*, Vol. 15, No. 3, 2001, pp. 308–316.

[28]Giordano, D., Capitelli, M., Colonna, G., and Gorse, C., "Tables of Internal Partition Functions and Thermodynamic Properties of High-Temperature Air Species," ESA Rept. STR-237, 1994.

[29]Biberman, L. M., Voro'ev, V. S., and Yakubov, I. T., "Elementary Processes in Low Temperature Plasma," *Kinetics of Nonequilibrium Low-Temperature Plasmas*, Consultants Bureau, New York, 1987.

[30]De Giacomo, A., Casavola, A., Colonna, G., De Pascale, O., and Capitelli, M., "Experimental and Theoretical Aspects of KrF Laser-Induced Plasma During Titanium Oxides Ablation," *Chemical and Physic News* (to be published).

[31]De Giacomo, A., Shakhatov, V. A., Senesi, G. S., and Orlando, S., "Spectroscopic Investigation of the Technique of Plasma Assisted Pulsed Laser Ablation of Titanium Dioxides," *Spectrochimica Acta Part B: Atomic Spectroscopy*, Vol. 56, No. 8, 2001, pp. 1459–1472.

[32]Wang, X. T., Man, B. Y., Wang, G. T., Zhao, Z., Xu, B. Z., Xia, Y. Y., Mei, L. M., and Hu, X. Y., "Optical Spectroscopy of Plasma Produced by Laser Ablation of Ti Alloy in Air," *Journal of Applied Physics*, Vol. 80, No. 3, 1996, pp. 1783–1786.

[33]Hermann, J., Thomann, A. L., Boulmer-Leborgne, C., Dubreuil, B., De Giorgi, M. L., Perrone, A., Luches, A., and Mihailescu, I. N., "Plasma Diagnostic in Pulsed Laser TiN Layer Deposition," *Journal of Applied Physics*, Vol. 77, No. 7, 1995, pp. 2928–2936.

[34]Amoruso, S., Armenante, M., Berardi, V., Bruzzese, R., and Spinelli, N., "Absorption and Saturation Mechanisms in Aluminium Laser Ablated Plasmas," *Applied Physics A: Material Science and Processing*, Vol. A65, No. 3, 1997, pp. 265–271.

[35]Kools, J. C. S., Baller, T. S., De Zwart, S. T., and Dieleman, J., "Gas Flow Dynamics in Laser Ablation Deposition," *Journal of Applied Physics*, Vol. 71, No. 9, 1992, pp. 4547–4556.

[36]Hermann, J., Boulmer-Leborgne, C., and Hong, D., "Diagnostics of Early Phase of an Ultraviolet Laser Induced Plasma Spectral Lines Analysis Considering Self-Absorption," *Journal of Applied Physics*, Vol. 83, No. 2, 1998, pp. 691–696.

[37]Capitelli, M., Capitelli, F., and Eletskii, A., "Non-Equilibrium and Equilibrium Problems in Laser-Induced Plasmas," *Spectrochimica Acta Part B: Atomic Spectroscopy*, Vol. 55B, No. 6, 2000, pp. 559–574.